

Zero Energy Heating of Solvent with Network-Structured Solar-Thermal Material: Eco-Friendly Palladium Catalysis of the Suzuki Reaction

Seungbeom Park, Woomin Park, Kangjoo Lee, Sun-Joon Min,* and Kwang-Suk Jang*



Cite This: *ACS Appl. Mater. Interfaces* 2022, 14, 40967–40974



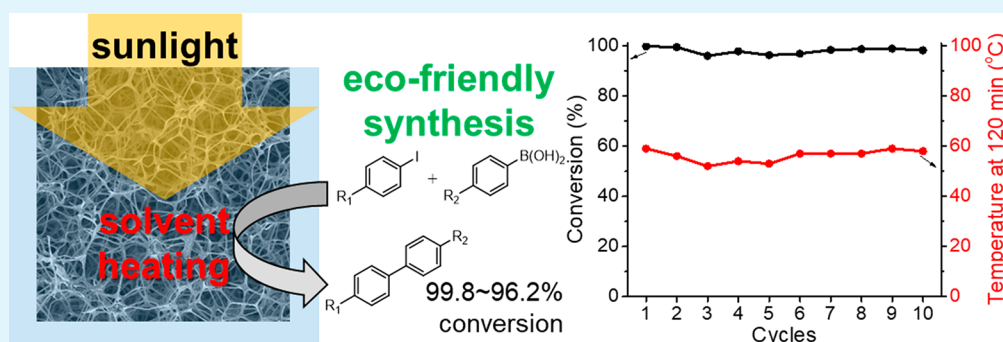
Read Online

ACCESS |

Metrics & More

Article Recommendations

Supporting Information



ABSTRACT: Solar-thermal materials absorb sunlight and convert it into heat, which is released into the surrounding medium. Utilization of solar energy for solvent heating can be a potential method of eco-friendly organic reactions. However, to date, significant heating of the entire volume of a solvent by 1 sun illumination has not been reported. In the present work, a network-structured solar-thermal material with an additional catalytic function was fabricated by sputtering palladium into a melamine sponge. The nanocrystalline palladium-decorated melamine sponge (Pd-sponge) has excellent sunlight absorption properties in the entire wavelength range that enable efficient solar-thermal conversion. The Pd-sponge can reduce heat loss to the surroundings by effectively blocking thermal radiation from the heated solvent. The temperature of the reaction solution with the ethanol–water mixture filled in the Pd-sponge increased from 23 to 59 °C under 1 sun illumination. The elevated temperature of the reaction solutions by solar-thermal conversion successfully accelerated the heterogeneous Pd-catalyzed Suzuki coupling reactions with high conversions. Easy and low-energy-consuming multicycle use of the solar-thermal and catalytic properties of the Pd-sponge has also been demonstrated.

KEYWORDS: solar-thermal effect, network structure, eco-friendly reaction, Pd catalyst, Suzuki reaction

INTRODUCTION

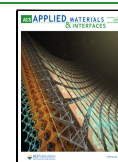
Photothermal materials absorb light on illumination and convert it into heat, which is released into the surrounding medium. Photothermal materials that absorb laser light of a specific wavelength can be used for cancer therapy through targeted cell ablation.^{1–7} Photothermal materials that absorb a wide range of wavelengths of sunlight, that is, solar-thermal materials, can be used for the desalination of seawater.^{8–14} Solar-thermal materials can generate heat by absorbing sunlight, a sustainable energy source, to enhance the evaporation rate of water molecules in seawater for collecting fresh water. For efficient solar-thermal desalination, a selective increase in the surface temperature of seawater has been most widely pursued by using various structures of solar-thermal materials. For example, solar-thermal materials with a porous film structure can effectively increase the surface temperature by floating in seawater.^{8–14}

Recently, the photothermal heating of solvents for chemical reactions has been proposed.^{15–20} In many cases, the chemical reactivity and reaction rate increase at higher temperatures. The conversion of light energy to heat can be utilized for solvent heating instead of the traditional methods that use fossil fuels or electricity. Particle-type photothermal materials have mostly been used for photothermal heating of solvents. The photothermal particles dispersed in a solvent dissipate the absorbed photon energy into heat to increase the solvent

Received: June 14, 2022

Accepted: August 18, 2022

Published: August 30, 2022



temperature. Higher conversions and reaction rates can be achieved by photothermal heating in organic reactions.^{15–19} Artificial high-power light using a laser or lamp is generally employed for volumetric heating of a solvent. Green chemistry along with cost reduction can be achieved via solvent heating by utilization of sunlight as a photon energy source. However, to date, significant heating of the entire volume of a solvent by 1 sun illumination has not been reported. Thus, the development of more efficient solar-thermal materials for zero energy heating of solvents is desirable. In addition, energy consumption can also be reduced by facilitating multicycle use of solar-thermal materials and catalysts for eco-friendly organic reactions. The key requirements for use of solar-thermal materials in eco-friendly organic reactions are suggested: (1) efficient solar-thermal conversion in the entire range of wavelengths of sunlight, (2) effective reduction of heat loss to the surroundings, (3) capability of acting as a catalyst support, and (4) easy and low-energy-consuming multicycle use.

In this study, the use of an open network structure of solar-thermal materials has been proposed to fulfill these key requirements. The network structure is advantageous for (1) reducing the loss of incident light by confining it within the network through multiple reflections and scattering, (2) reducing heat loss to the surroundings by effectively blocking thermal radiation from the heated solvent, (3) supporting catalytic components allowing facile contact with reactants, and (4) easy and low-energy-consuming separation from the reaction solution for multicycle use. The network-structured solar-thermal material was fabricated by the growth of nanocrystalline palladium on the skeleton of a melamine sponge. Since nanocrystalline palladium acts as an outstanding catalyst in a wide variety of organic syntheses as well as a good light absorber, the nanocrystalline palladium-decorated sponge (Pd-sponge) has both solar-thermal and catalytic properties. Effective volumetric heating of a solvent for organic reaction is attainable by 1 sun illumination of the Pd-sponge filled with solvent. For example, the temperatures of the ethanol–water mixture (1:1 volume ratio) and dimethylformamide increased from 23 to 57 °C and 23 to 67 °C, respectively, by solar-thermal conversion. Pd-catalyzed Suzuki coupling reactions were accelerated by solar-thermal heating of the reaction solutions with an ethanol–water mixture. The easy and low-energy-consuming multicycle use of the solar-thermal and catalytic Pd-sponge has also been demonstrated. This study introduces network-structured solar-thermal materials for application in low-energy eco-friendly organic reactions.

RESULTS AND DISCUSSION

The Pd-sponge was prepared by sputtering palladium onto a melamine sponge. Because the sputtering depth of palladium into the melamine sponge is ~ 1 mm, palladium was sputtered on both sides of the melamine sponge with a thickness of 2 mm. By stacking up the 2 mm thick single layers, the overall layer thickness of the Pd-sponge can be controlled. The pore volume fraction of the Pd-sponge was measured to be more than 95%. The solvent was filled overall into the Pd-sponge, and sunlight was illuminated for solvent heating by solar-thermal conversion (Figure 1). With the sputtering of palladium, the color of the sponge changed from white to black (Figure 2a). The weight content of palladium in the Pd-sponge was determined to be 3.1% by inductively coupled plasma-mass spectrometry (ICP-MS). A dramatic color change

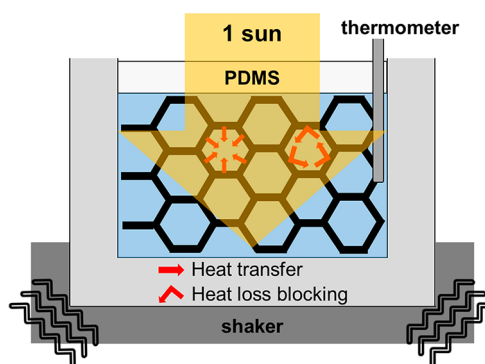


Figure 1. Schematic for the solar-thermal heating of solvent with the Pd-sponge.

was caused by the small amount of palladium. Figure 2b–f shows the scanning electron microscope (SEM) images of the melamine sponge and Pd-sponge. In the low-magnification images, no morphological differences were observed between the two samples (Figure 2b,d). By sputtering, palladium particles with a length of ~ 40 nm and a width of ~ 20 nm were coated on the melamine skeleton (Figure 2c,e,f). To obtain a transmission electron microscope (TEM) image, the palladium particles were detached from the Pd-sponge by sonication in ethanol. Crystal grain sizes of less than 7 nm can be observed in the TEM image (Figure 2g). Figure 2h shows the X-ray diffraction (XRD) patterns of the melamine sponge and Pd-sponge. The two broad peaks at 12° and 22° are attributed to the melamine polymer. Other peaks of the Pd-sponge are in accordance with the PDF card (9013416) data for palladium. Owing to the low content and small crystal grain size of palladium, small and broad XRD peaks were obtained. The presence of metallic Pd in the Pd-sponge was also verified by X-ray photoelectron spectroscopy (XPS) analysis (Figure 2i). The Pd 3d_{5/2} peaks at 335.9 and 337.4 eV can be attributed to Pd⁰ and Pd²⁺, respectively. Metallic palladium is the major phase with a Pd⁰ ratio of 80% in the Pd-sponge.

For efficient solar-thermal conversion, the entire range of wavelengths of sunlight should be absorbed effectively. This can be accomplished by the use of an ideal blackbody material as a light absorber or a proper material structure to effectively increase the absorption and reduce the loss of incident sunlight. Figure 3a–c shows the transmittance, reflectance, and absorption spectra of the Pd-sponges with overall layer thicknesses of 2–16 mm in the wavelength range of 280–2500 nm, which corresponds to the main wavelength range of sunlight. On illumination into the 2 mm thick Pd-sponge, 5.1% to 7.1% of the light was transmitted (Figure 3a). When light is illuminated into the thicker Pd-sponge, the transmittance reduced to near zero over the entire wavelength range (Figure 3a). However, the reflectance was not affected by the overall layer thickness of the Pd-sponge (Figure 3b). These results indicate that the total absorption of sunlight increases efficiently by increasing the Pd-sponge thickness without additional loss by reflectance. The network structure is advantageous for reducing the loss of incident light, which can be confined within the network through multiple light reflections and scattering. The light confined within the network will eventually be absorbed by the solar-thermal material. To show the effect of the network structure on light absorption, a compressed Pd-sponge that lost the original network structure was also prepared (Figure S1). By hot-

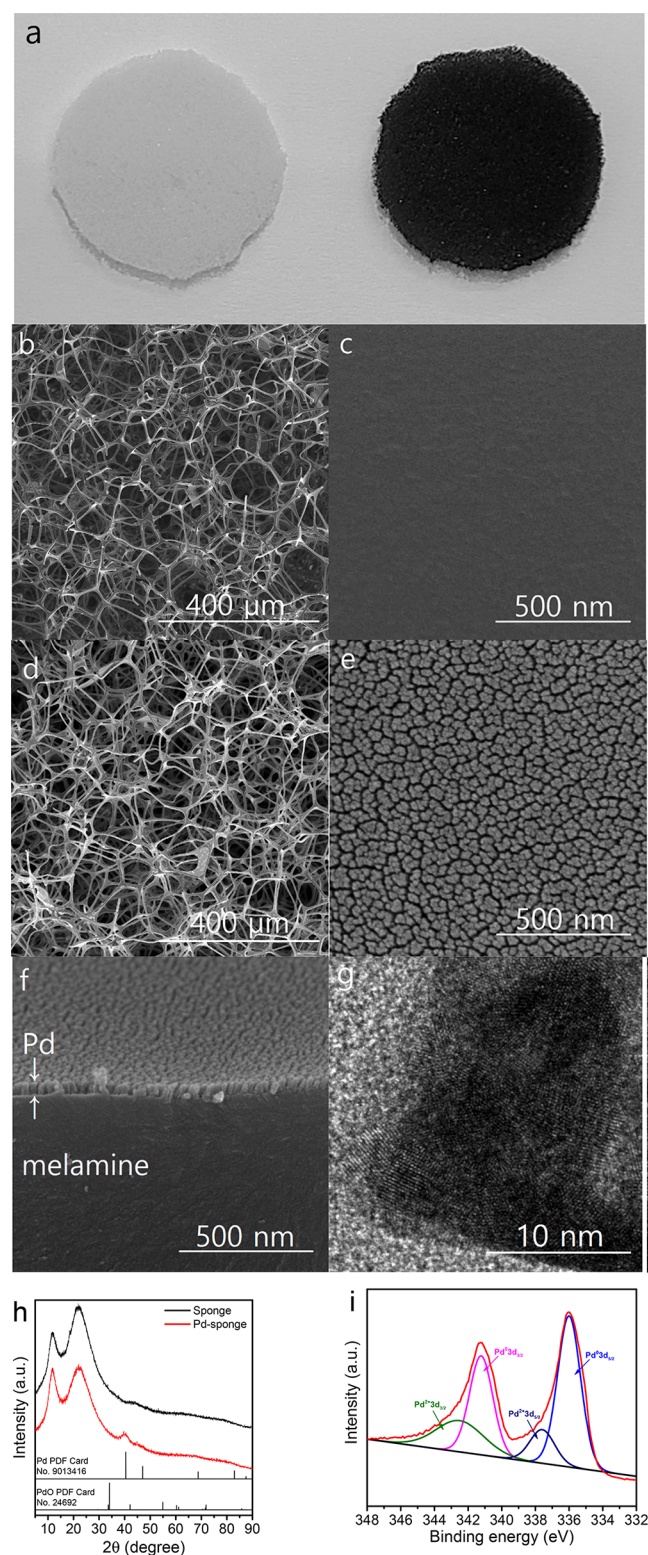


Figure 2. (a) Photograph of the melamine sponge (white) and Pd-sponge (black). SEM images of the (b),(c) melamine sponge and (d),(e),(f) Pd-sponge. (g) TEM image of the palladium particle detached from the Pd-sponge. (h) XRD patterns of the melamine sponge and Pd-sponge. (i) Pd 3d XPS spectrum of the Pd-sponge.

pressing at 230 °C and 1 MPa for 10 min, a Pd-sponge with a thickness of 2 mm was compressed to a thickness of 0.33 mm. The Pd-sponge showed lower transmittance and reflectance than the compressed Pd-sponge (Figure S2). These results

confirm the confinement of incident light within the Pd-sponge network. By using the transmittance and reflectance values, the absorption spectra of the Pd-sponges were obtained (Figure 3c). For effective sunlight absorption, an overall layer thickness of 4 mm or more is required since the absorption at 500 nm was saturated when the overall layer thickness of the Pd-sponge was over 4 mm (Figure 3d). The absorbance values of the Pd-sponges with an overall layer thickness of 4 mm or more ranged from 91% to 99% over the entire wavelength range. Despite the low palladium content, the Pd-sponge shows excellent sunlight absorption properties originating from its network structure.

The Pd-sponge absorbs sunlight and converts it into heat which is released into the surrounding solvent. To increase the solvent temperature effectively, the heat loss of the solvent to the outside should be reduced. Thermal radiation is one of the major mechanisms of heat loss. The wavelength of thermal radiation from a material heated at below 500 K is typically in the range of 2500–25000 nm.²¹ The wavelength at the peak radiation can be estimated by using Wien's displacement law, $\lambda_{\text{max}} = b/T$, where b and T are Wien's displacement constant, 2.98×10^{-3} m K, and absolute temperature, respectively.²² For example, the peak wavelengths of thermal radiation from the material heated at temperatures of 293, 323, and 353 K were estimated to be 10200, 9230, and 8440 nm, respectively. Thermal radiation in the wavelength range of 2500–25000 nm cannot transmit 4 mm or more of the Pd-sponge, according to the IR transmittance spectra (Figure 3e). Thus, the Pd-sponge can reduce heat loss to the surroundings by effectively blocking thermal radiation from the heated solvent. The near-zero IR transmittance might originate from the multiple reflections and absorptions of IR light by the skeletons of the Pd-sponge. Because all parts of the solvent filled in the Pd-sponge are surrounded by the network, the thermal radiation in all directions can be effectively blocked.

The nanocrystalline palladium grown on the melamine sponge can act as both a light absorber and a catalyst for organic reactions. The use of nanocrystalline palladium as a heterogeneous catalyst in various liquid-phase reactions is very common in academia and industry.^{23–27} The network structure leads to facile contact between the nanocrystalline palladium and the reaction solution, filling the Pd-sponge with a pore volume fraction of more than 95%. In addition to nanocrystalline palladium, other catalytic components can be attached to the Pd-sponge. After the synthesis process, the reaction solution was collected by gentle squeezing of the Pd-sponge. Further separation of the light absorber and catalyst was not required. Thus, the energy consumption for separation can be reduced by using the Pd-sponge. Figure 3f shows the compressive stress–strain curves of the Pd-sponge at a set maximum strain of 60% for 10 cycles. The Pd-sponge was found to be highly elastic with perfect shape recovery after 10 cycles of compression.

Heat from the heated solvent can be lost by radiation, evaporation, convection, and conduction. Heat loss by radiation can be effectively reduced by the presence of a network-structured Pd-sponge. To reduce heat loss by evaporation, convection, and conduction, a polydimethylsiloxane (PDMS) layer with a thickness of 2.5 mm was introduced on top of the Pd-sponge (Figure 1). PDMS is a transparent elastomer with a low thermal conductivity. Figure S3 shows the transmittance spectrum of the 2.5 mm thick PDMS in the wavelength range of 280 to 2500 nm, where wavelength

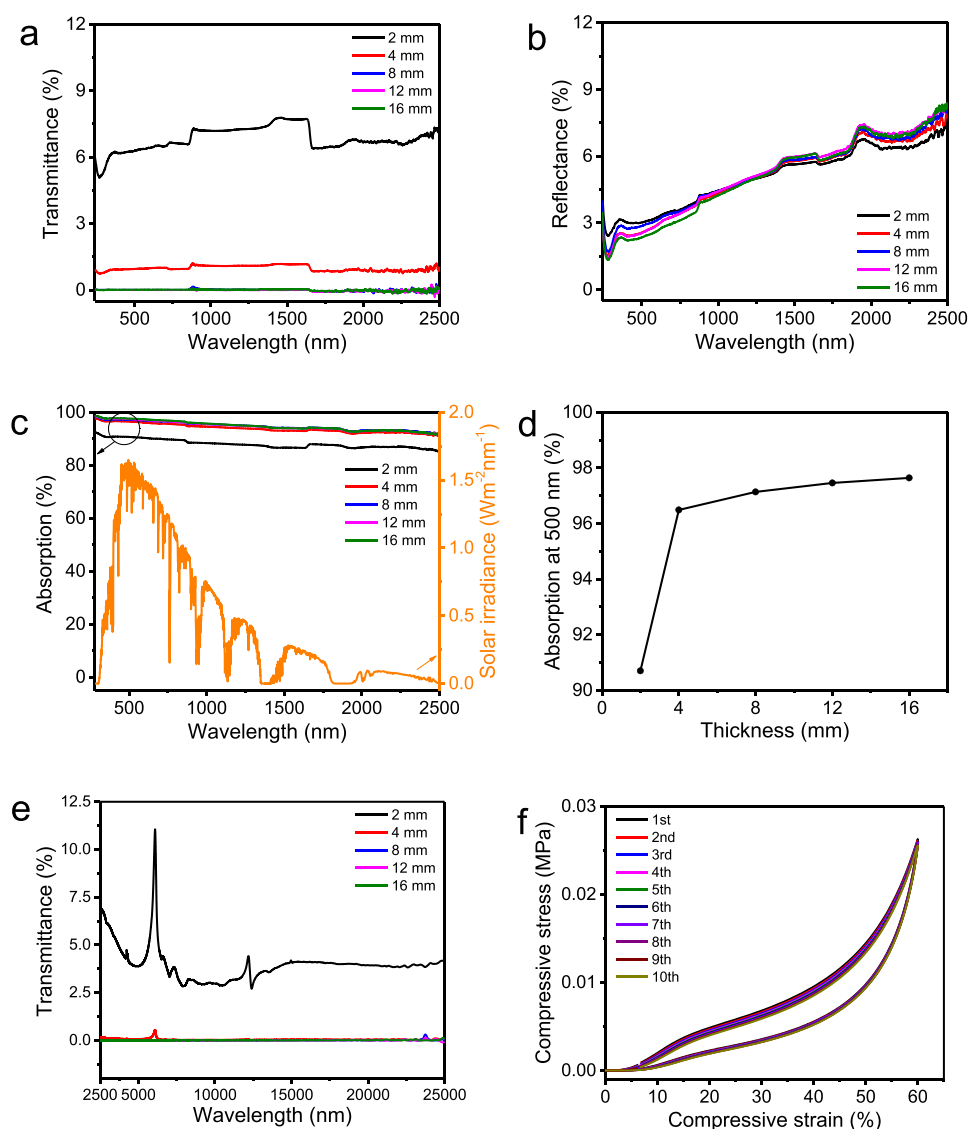


Figure 3. UV-vis-NIR (a) transmittance, (b) reflectance, and (c) absorption spectra of the Pd-sponges with thicknesses of 2 to 16 mm. For comparison, the standard solar radiation spectra of air mass 1.5 global (AM 1.5G) is also illustrated in (c). (d) Thickness-dependent absorption of the Pd-sponges at 500 nm. (e) IR transmittance spectra of the Pd-sponges with thicknesses of 2 to 16 mm. (f) Compressive stress–strain curves of the Pd-sponge with a thickness of 12 mm for 10 cycles.

regions with a transmittance of more than 90% are highlighted in gray. PDMS has relatively low transmittance values in some IR regions. However, a large portion of sunlight, including the wavelength range of 320 to 1150 nm, will reach the Pd-sponge for solar-thermal conversion. Additionally, because of the elastic properties of PDMS, the reaction solution can be perfectly sealed. Thus, evaporation of the solvent will be blocked, and the effect of convection of the outside air can be eliminated. Because the thermal conductivity of the PDMS layer with a thickness of 2.5 mm was measured to be as low as 0.166 and 0.154 $\text{W m}^{-1} \text{K}^{-1}$ at 25 and 55 $^{\circ}\text{C}$, respectively (Table S1), heat loss by conduction from the heated solvent can be reduced significantly. Hence, by using the PDMS top layer, it is expected that the heat loss by evaporation, convection, and conduction can be effectively reduced.

To show zero energy heating of the solvent by solar-thermal conversion, the Pd-sponge, fully filled with solvent and sealed by the PDMS top layer, was exposed under AM 1.5 G simulated solar illumination with an intensity of 100 mW cm^{-2}

(Figure 1). Figure 4a shows the illumination time-dependent temperature of the ethanol–water mixture (1:1 volume ratio) in the presence of and absence of the 12 mm thick Pd-sponge. The solution temperature reached 57 $^{\circ}\text{C}$ within 120 min of simulated sunlight illumination by solar-thermal conversion of the Pd-sponge. Without the Pd-sponge, the temperature of the ethanol–water mixture can reach only 37 $^{\circ}\text{C}$ under simulated sunlight illumination. Since the solvent was shaken during illumination, there was a negligible temperature difference along the penetration depth of the thermometer. The overall layer thickness of the Pd-sponge with a pore volume fraction of more than 95% determines the total volume of the solvent. Thus, the total heat capacity of the filled solvent increases in direct proportion to the overall layer thickness of the Pd-sponge. When considering sunlight absorption, a thickness of only 4 mm was sufficient. However, for the optimized reduction of heat loss by thermal radiation, a larger thickness might be advantageous. For example, a penetration depth of more than 4 mm is required for perfect blocking of thermal

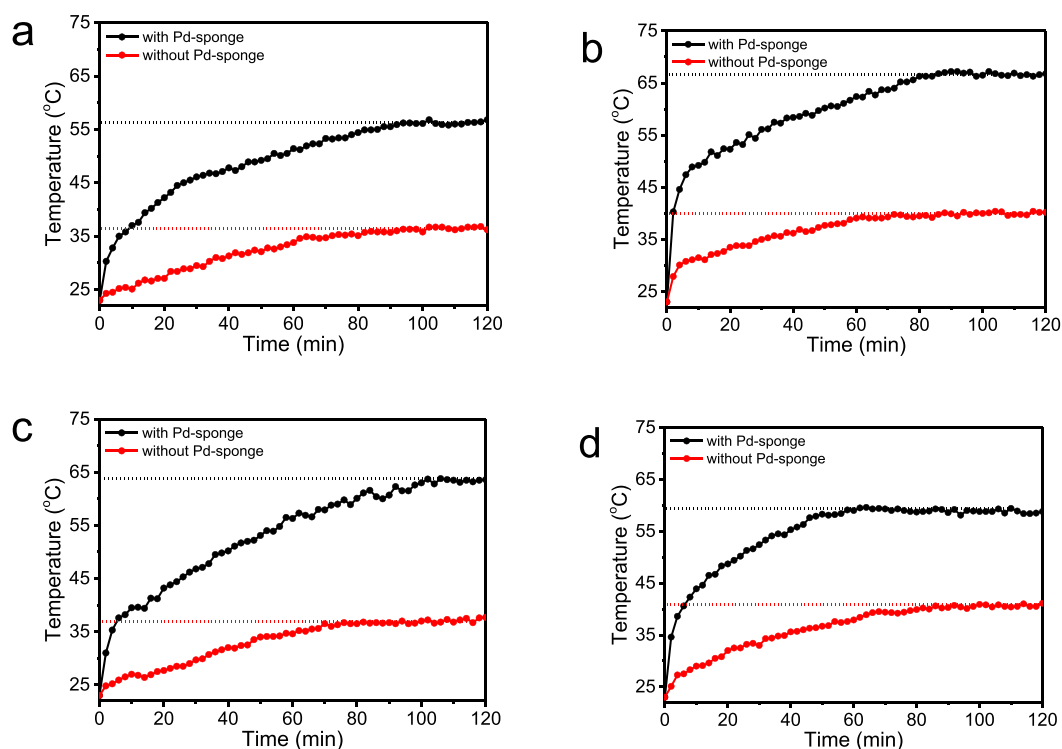
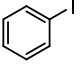
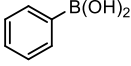
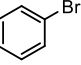
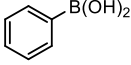
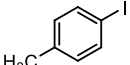
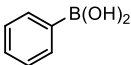
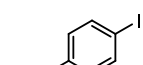
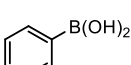
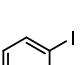
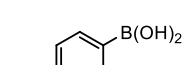
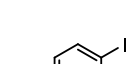
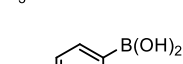
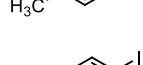
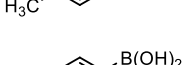


Figure 4. Illumination time-dependent temperatures of the (a) ethanol–water mixture (1:1 volume ratio), (b) dimethylformamide, (c) ethanol, and (d) the model reaction solution in the presence and absence of the Pd-sponge.

Table 1. Conversions of the Suzuki Coupling Reactions in the Presence of the Pd-Sponge under Simulated Sunlight Illumination

entry	halide	boronic acid	temperature at 120 min (°C)	conversion ^a (%)
1			59 (23 ^b)	99.8 (5.4 ^b)
2			58	96.2
3			57	98.3
4			58	99.7
5			57	99.9
6			58	99.8
7			60	99.8

^aConversion calculated from the molar ratio of the limiting reactant to the product determined by GC-MS analysis. ^bReaction under dark conditions for comparison.

radiation to the top surface. Figure S4 shows the Pd-sponge thickness-dependent temperature of the ethanol–water mixture (1:1 volume ratio) at 120 min of simulated sunlight illumination. The overall layer thickness of the Pd-sponge was optimized at 12 mm for the highest temperature of the ethanol–water mixture. Figure S5 shows the illumination time-dependent temperature of the ethanol–water mixture (1:1 volume ratio) in the presence of the compressed Pd-sponge with an original thickness of 12 mm. The solution temperature reached a lower temperature of 52 °C due to lower light absorption ability of the compressed Pd-sponge. Photothermal conversion efficiency is expressed as the percentage ratio of $C_p m \Delta T$ to $I \Delta t$, where C_p , m , ΔT , I , and Δt are specific heat capacity, mass of the solvent, temperature difference, light intensity, and illumination time, respectively. Photothermal conversion efficiencies during the 120 min of simulated sunlight illumination by solar-thermal conversion of the pristine and compressed Pd-sponge are calculated to be 20% and 17%, respectively. In addition to the ethanol–water mixture, various solvents can be heated by solar-thermal conversion of the Pd-sponge (Figure 4b,c). The temperatures of dimethylformamide and ethanol reached 67 and 64 °C, respectively, by solar-thermal conversion of the Pd-sponge. Without the Pd-sponge, the temperatures of dimethylformamide and ethanol could reach only 40 and 38 °C, respectively, under simulated sunlight illumination.

To demonstrate eco-friendly organic reactions by zero energy heating of the solvent with the Pd-sponge, heterogeneous Pd-catalyzed Suzuki coupling reactions were performed (Table 1). The Suzuki coupling reaction is the most useful synthetic process in organic chemistry for forming C–C bonds across industry and academia.^{28–33} As a model reaction, the Suzuki coupling reaction of iodobenzene and phenylboronic acid was performed using an environmentally benign ethanol–water mixture (1:1 volume ratio) as the reaction solvent. The temperature of the reaction solution filled in the Pd-sponge reached 59 °C after 60 min of simulated sunlight illumination (Figure 4d). Without the Pd-sponge, the temperature of the reaction solution could reach only 41 °C under simulated sunlight illumination. The reaction produces biphenyl with a high conversion of 99.8%, which was calculated from the molar ratio of the limiting reactant to the product determined by GC-MS analysis. The reaction product was separated with a yield of 91.9%, and its structure was confirmed by the analysis of ¹H and ¹³C NMR spectra (Figure S6). For comparison, the reaction was performed under dark conditions. A much lower conversion of 5.4% was obtained by the reaction at an unchanged temperature of 23 °C. These results indicate that the solar-thermal heating of the reaction solution accelerates the model reaction. A difference in the XRD pattern and Pd 3d XPS spectrum of the Pd-sponges before and after the model reaction is not observed (Figures S7 and S8). The metallic Pd⁰ ratio of 80% in the Pd-sponge is unchanged after the model reaction. For comparison, the model reactions were also performed with the commercially available palladium on a carbon (Pd/C) catalyst by using the conventional solvent heating method with an oil bath. The reactions produce biphenyl with conversions of 6.2% and 99.9% at 23 and 60 °C, respectively. For further demonstrations, more Suzuki coupling reactions were performed (Table 1). The elevated temperatures of the reaction solutions by solar-thermal conversion, ranging from 57 to 60 °C, accelerate the reactions with high conversion ranging from 96.2% to 99.9%. Figure S9 shows our

proposed mechanism for the Suzuki reaction catalyzed by the Pd-sponge. The C–I group of the aryl halide molecule can be absorbed on the nanocrystalline Pd, which serves as the electron donation site to weaken the C–I bond. The subsequent reductive elimination and transmetalation occur to form the reaction product. The multicycle usability of the Pd-sponge was tested in the Suzuki coupling reaction of iodobenzene and phenylboronic acid (Figure 5). The Pd-

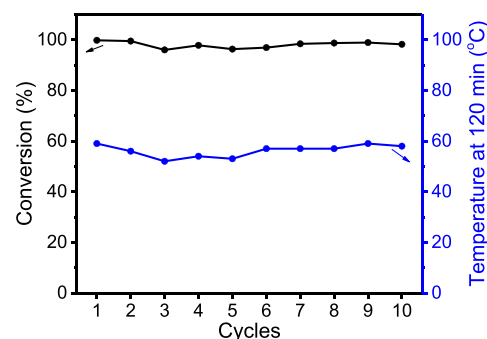


Figure 5. Multicycle usability test of the Pd-sponge in the Suzuki coupling reaction of iodobenzene and phenylboronic acid.

sponge could be successfully used for 10 runs without any considerable loss in solar-thermal and catalytic activities for the Suzuki coupling reaction. During the consecutive 10 runs, the elevated temperatures of the reaction solutions ranging from 54 to 59 °C accelerate the reactions with conversions ranging from 96.0% to 99.8%. Because the Pd-sponge can be easily separated from the reaction solution, it is expected that the energy consumption for separation can be reduced significantly. The easy and low-energy-consuming multicycle use of the solar-thermal and catalytic properties of the Pd-sponge was demonstrated by the multicycle test. The present work is the proof of concept of the solar-thermal solvent heating for eco-friendly organic reactions. In this study, Pd is used as both a light absorber and a catalyst for organic reactions. We anticipate that more inexpensive light-absorbing materials such as carbon and conjugated polymers can be used instead of Pd. We also anticipate that the solar-thermal heating can be applied to various organic reactions.

CONCLUSIONS

The zero energy heating of a solvent has been demonstrated with a network-structured Pd-sponge by converting sunlight to heat. A solar-thermal Pd-sponge with an additional catalytic feature was fabricated by sputtering palladium into the melamine sponge. The Pd-sponge leads to efficient solar-thermal conversion in the entire range of wavelengths of sunlight and effective blocking of thermal radiation from the heated solvent to decrease heat loss to the surroundings. By solar-thermal heating of the reaction solution filled in the Pd-sponge, heterogeneous Pd-catalyzed Suzuki coupling reactions were successfully accelerated. Because the reaction solution can be collected from the Pd-sponge by gentle squeezing, the solar-thermal and catalytic properties of the Pd-sponge can be exploited repeatedly with ease and low-energy consumption. The results suggest that utilization of network-structured solar-thermal materials can be a potential method of low-energy eco-friendly organic reactions.

METHODS

Preparation and Characterization of the Pd-Sponge. Before use, the melamine sponge (Basotect G+, BASF) was washed with deionized water and ethanol and then dried at 60 °C for more than 2 h. The Pd-sponge was prepared by sputtering Pd into the melamine sponge with a diameter of 20 mm and a thickness of 2 mm using an ion-sputter (G20, GSEM). The deposition was performed at 5 mA for 40 min. The weight content of palladium in the Pd-sponge was measured by ICP-MS (iCAP RQ, Thermo Fisher Scientific). The SEM images were recorded using a field-emission SEM (Nova NanoSEM450, FEI). The TEM image was recorded using a field emission TEM (Tecnai G2 F20, FEI) operating at 200 kV. The XRD patterns were obtained using an X-ray diffractometer (Miniflex600, Rigaku) equipped with Cu K α radiation ($\lambda = 1.5406 \text{ \AA}$) at 40 kV and 15 mA. The XPS analysis was performed using an X-ray photoelectron spectrometer (K-Alpha+, Thermo Fisher Scientific). The reflectance, transmittance, and absorption spectra in the wavelength range of 280–2500 nm were obtained using an ultraviolet–visible–near-infrared (UV–vis–NIR) spectrometer (SolidSpec-3700, Shimadzu). The transmittance spectra in the wavelength range of 2500–25000 nm were obtained using a Fourier transform infrared spectrometer (Nicolet iS50, Thermo Fisher Scientific). The compressive stress–strain curves were obtained using a micromechanical test (model: 5848, Instron).

Preparation and Characterization of PDMS. The PDMS base polymer and curing agent (Sylgard 184, Dow Corning) were mixed in a weight ratio of 12:1. The mixture was then poured into a Petri dish and annealed at 80 °C for 1 h. The thermal diffusivity (λ) of the PDMS was measured using a laser flash thermal analyzer (LFA 467, Netzsch) at 25 and 55 °C. The heat capacity (C_p) was measured by differential scanning calorimetry (DSC 200 F3, Netzsch). Thermal conductivity was calculated from the relationship $\kappa = d\lambda C_p$, where d is the density.

Solar-Thermal Heating of Solvent. A Pd-sponge with an overall thickness of 12 mm was loaded in a Teflon cylindrical vessel with a diameter of 20 mm. Subsequently, 4.3 mL of solvent was filled in the Pd-sponge and sealed by the PDMS top layer. The AM 1.5 G simulated sunlight with an intensity of 100 mW cm⁻² was illuminated using a Xe lamp solar simulator (model: 10500, ABET Technologies). During the 2 h illumination, the vessel was constantly shaken using a mini orbital shaker (VM-96T, Lab Companion) at 350 rpm. The temperature of the solvent was measured using a tip-type thermometer (model: 108, type T thermometer, Testo).

Suzuki Coupling Reactions. In 4.3 mL of an ethanol-deionized water mixture with a 1:1 volume ratio, 0.4 mmol of aryl halide, 0.48 mmol of arylboronic acid, and 1.2 mmol of K₂CO₃ were added. The reaction solution was filled in the Pd-sponge with an overall thickness of 12 mm loaded in a Teflon vessel and sealed with PDMS. During 2 h illumination of the simulated sunlight, the vessel was constantly shaken at 350 rpm. Then, the reaction solution was collected by gentle squeezing of the Pd-sponge. For the multicycle test, the Pd-sponge was squeezed for recovery from the reaction solution, washed with deionized water and ethanol, and then dried at 60 °C for more than 2 h after each reaction cycle. The dried Pd-sponge was reused for the next reaction cycle. Conversion of each reaction cycle was analyzed using a GC-MS system. The crude reaction product was extracted with ethyl acetate and immediately analyzed using a gas chromatography–mass spectroscopy (GC-MS) system (model: 7890B and 5977B, Agilent). For isolation, the reaction mixture was quenched with saturated aqueous NH₄Cl, extracted with diethyl ether, and washed with brine. The combined organic layers were dried over anhydrous MgSO₄ and concentrated *in vacuo*. The resulting residue was purified by flash column chromatography on silica gel (petroleum ether = 100) to afford the target compound (57.1 mg, 91.9%) as a white solid. The ¹H and ¹³C nuclear magnetic resonance (NMR) spectra were recorded on a Bruker 400 MHz instrument using CDCl₃ as the NMR solvent. For comparison of the catalytic performance, 0.1 mol % of Pd/C with a Pd content of 5 wt % (Sigma-Aldrich) was used in the model reaction.

ASSOCIATED CONTENT

Supporting Information

The Supporting Information is available free of charge at <https://pubs.acs.org/doi/10.1021/acsami.2c10530>.

Details for the calculation of thermal conductivities of the PDMS, photograph and SEM images of the compressed Pd-sponge, UV–vis–NIR transmittance, reflectance, and absorption spectra of the pristine and compressed Pd-sponges, UV–vis–NIR transmittance spectrum of the PDMS, Pd-sponge thickness-dependent temperature of the ethanol–water mixture at 120 min of simulated sunlight illumination, and ¹H and ¹³C NMR spectra of biphenyl (PDF)

AUTHOR INFORMATION

Corresponding Authors

Sun-Joon Min – Department of Applied Chemistry and Center for Bionano Intelligence Education and Research, Hanyang University, Ansan, Gyeonggi-do 15588, Republic of Korea; orcid.org/0000-0003-0867-4416; Email: sjmin@hanyang.ac.kr

Kwang-Suk Jang – Department of Applied Chemistry and Center for Bionano Intelligence Education and Research, Hanyang University, Ansan, Gyeonggi-do 15588, Republic of Korea; orcid.org/0000-0001-5835-9364; Email: kjang@hanyang.ac.kr

Authors

Seungbeom Park – Department of Applied Chemistry and Center for Bionano Intelligence Education and Research, Hanyang University, Ansan, Gyeonggi-do 15588, Republic of Korea

Woomin Park – Department of Applied Chemistry and Center for Bionano Intelligence Education and Research, Hanyang University, Ansan, Gyeonggi-do 15588, Republic of Korea

Kangjoo Lee – Department of Applied Chemistry and Center for Bionano Intelligence Education and Research, Hanyang University, Ansan, Gyeonggi-do 15588, Republic of Korea

Complete contact information is available at: <https://pubs.acs.org/doi/10.1021/acsami.2c10530>

Funding

This work was supported by the Basic Research Program through the National Research Foundation of Korea (NRF) funded by the MSIT (2020R1A4A4079870) and the GRRC program of Gyeonggi province (GRRCHanyang2020-B01).

Notes

The authors declare no competing financial interest.

REFERENCES

- Wang, P.; Kankala, R. K.; Chen, B.; Zhang, Y.; Zhu, M.; Li, X.; Long, R.; Yang, D.; Krastev, R.; Wang, S.; Xiong, X.; Liu, Y. Cancer Cytochrome-Cloaked Prussian Blue Nanoparticles Enhance the Efficacy of Mild-Temperature Photothermal Therapy by Disrupting Mitochondrial Functions of Cancer Cells. *ACS Appl. Mater. Interfaces* **2021**, *13*, 37563–37577.
- Zhao, Y.; Zhao, T.; Cao, Y.; Sun, J.; Zhou, Q.; Chen, H.; Guo, S.; Wang, Y.; Zhen, Y.; Liang, X.-J.; Zhang, S. Temperature-Sensitive Lipid-Coated Carbon Nanotubes for Synergistic Photothermal Therapy and Gene Therapy. *ACS Nano* **2021**, *15*, 6517–6529.
- Liu, Y.; Li, H.; Li, S.; Zhang, X.; Xiong, J.; Jiang, F.; Liu, Y.; Jiang, P. Chiral Cu_{2-x}Se Nanoparticles for Enhanced Synergistic Cancer

- Chemodynamic/Photothermal Therapy in the Second Near-Infrared Biowindow. *ACS Appl. Mater. Interfaces* **2021**, *13*, 60933–60944.
- (4) Biutty, M. N.; Zakia, M.; Yoo, S. I. Enhanced Photothermal Heating from One-dimensional Assemblies of Au Nanoparticles Encapsulated by TiO₂ Shell. *Bull. Korean Chem. Soc.* **2020**, *41*, 1033–1039.
- (5) Choi, W.; Sahu, A.; Kim, Y.; Tae, G. Photothermal Cancer Therapy and Imaging Based on Gold Nanorods. *Ann. Biomed. Eng.* **2012**, *40*, 534–546.
- (6) Li, X.; Lovell, J. F.; Yoon, J.; Chen, X. Clinical Development and Potential of Photothermal and Photodynamic Therapies for Cancer. *Nat. Rev. Clin. Oncol.* **2020**, *17*, 657–674.
- (7) Zhi, D.; Yang, T.; O'Hagan, J.; Zhang, S.; Donnelly, R. F. Microneedles for Photodynamic and Photothermal Therapy. *J. Controlled Release* **2020**, *325*, 52–71.
- (8) Liu, X.; Tian, Y.; Wu, Y.; Chen, F.; Mu, Y.; Minus, M. L.; Zheng, Y. Fully Biomass-Based Hybrid Hydrogel for Efficient Solar Desalination with Salt Self-Cleaning Property. *ACS Appl. Mater. Interfaces* **2021**, *13*, 42832–42842.
- (9) Peng, B.; Gao, Y.; Lyu, Q.; Xie, Z.; Li, M.; Zhang, L.; Zhu, J. Cationic Photothermal Hydrogels with Bacteria-Inhibiting Capability for Freshwater Production via Solar-Driven Steam Generation. *ACS Appl. Mater. Interfaces* **2021**, *13*, 37724–37733.
- (10) Yan, B.; Zhou, M.; Liao, X.; Wang, P.; Yu, Y.; Yuan, J.; Wang, Q. Developing a Multifunctional Silk Fabric with Dual-Driven Heating and Rapid Photothermal Antibacterial Abilities Using High-Yield MXene Dispersions. *ACS Appl. Mater. Interfaces* **2021**, *13*, 43414–43425.
- (11) Lu, Y.; Fan, D.; Wang, Y.; Xu, H.; Lu, C.; Yang, X. Surface Patterning of Two-Dimensional Nanostructure-Embedded Photothermal Hydrogels for High-Yield Solar Steam Generation. *ACS Nano* **2021**, *15*, 10366–10376.
- (12) Ma, C.; Liu, Q.; Peng, Q.; Yang, G.; Jiang, M.; Zong, L.; Zhang, J. Biomimetic Hybridization of Janus-like Graphene Oxide into Hierarchical Porous Hydrogels for Improved Mechanical Properties and Efficient Solar Desalination Devices. *ACS Nano* **2021**, *15*, 19877–19887.
- (13) Pang, Y.; Zhang, J.; Ma, R.; Qu, Z.; Lee, E.; Luo, T. Solar-Thermal Water Evaporation: A Review. *ACS Energy Lett.* **2020**, *5*, 437–456.
- (14) Liu, H.; Huang, Z.; Liu, K.; Hu, X.; Zhou, J. Interfacial Solar-to-Heat Conversion for Desalination. *Adv. Energy Mater.* **2019**, *9*, 1900310.
- (15) Yang, Q.; Xu, Q.; Yu, S.-H.; Jiang, H.-L. Pd Nanocubes@ZIF-8: Integration of Plasmon-Driven Photothermal Conversion with a Metal-Organic Framework for Efficient and Selective Catalysis. *Angew. Chem. Int. Ed.* **2016**, *55*, 3685–3689.
- (16) Wang, F.; Huang, Y.; Chai, Z.; Zeng, M.; Li, Q.; Wang, Y.; Xu, D. Photothermal-Enhanced Catalysis in Core-Shell Plasmonic Hierarchical Cu₇S₄ Microsphere@Zeolitic Imidazole Framework-8. *Chem. Sci.* **2016**, *7*, 6887–6893.
- (17) Ma, H.-C.; Zhao, C.-C.; Chen, G.-J.; Dong, Y.-B. Photothermal Conversion Triggered Thermal Asymmetric Catalysis within Metal Nanoparticles Loaded Homochiral Covalent Organic Framework. *Nat. Commun.* **2019**, *10*, 3368.
- (18) Wang, F.; Li, C.; Chen, H.; Jiang, R.; Sun, L.-D.; Li, Q.; Wang, J.; Yu, J. C.; Yan, C.-H. Plasmonic Harvesting of Light Energy for Suzuki Coupling Reactions. *J. Am. Chem. Soc.* **2013**, *135*, 5588–5601.
- (19) Chuang, C.-C.; Chu, H.-C.; Huang, S.-B.; Chang, W.-S.; Tuan, H.-Y. Laser-Induced Plasmonic Heating in Copper Nanowire Fabric as a Photothermal Catalytic Reactor. *Chem. Eng. J.* **2020**, *379*, 122285.
- (20) Pandres, E. P.; Crane, M. J.; Davis, J.; Pauzauskie, P. J.; Holmberg, V. C. Laser-Driven Growth of Semiconductor Nanowires from Colloidal Nanocrystals. *ACS Nano* **2021**, *15*, 8653–8662.
- (21) Halliday, D.; Resnick, R. *Fundamentals of Physics*; John Wiley & Sons, 1998.
- (22) Quinn, T. J. *Monographs in Physical Measurement: Temperature*; Academic Press, 1984.
- (23) Chen, Y. H.; Hung, H. H.; Huang, M. H. Seed-Mediated Synthesis of Palladium Nanorods and Branched Nanocrystals and Their Use as Recyclable Suzuki Coupling Reaction Catalysts. *J. Am. Chem. Soc.* **2009**, *131*, 9114–9121.
- (24) Chen, A. C.; Ostrom, C. Palladium-Based Nanomaterials: Synthesis and Electrochemical Applications. *Chem. Rev.* **2015**, *115*, 11999–12044.
- (25) Favier, I.; Pla, D.; Gómez, M. Palladium Nanoparticles in Polyols: Synthesis, Catalytic Couplings, and Hydrogenations. *Chem. Rev.* **2020**, *120*, 1146–1183.
- (26) Shi, W.; Niu, Y.; Li, S.; Zhang, L.; Zhang, Y.; Botton, G. A.; Wan, Y.; Zhang, B. Revealing the Structure Evolution of Heterogeneous Pd Catalyst in Suzuki Reaction via the Identical Location Transmission Electron Microscopy. *ACS Nano* **2021**, *15*, 8621–8637.
- (27) Nazemi, M.; Panikkanvalappil, S. R.; Liao, C.-K.; Mahmoud, M. A.; El-Sayed, M. A. Role of Femtosecond Pulsed Laser-Induced Atomic Redistribution in Bimetallic Au–Pd Nanorods on Optoelectronic and Catalytic Properties. *ACS Nano* **2021**, *15*, 10241–10252.
- (28) Miyaura, N.; Yamada, K.; Suzuki, A. A New Stereospecific Cross-Coupling by the Palladium-Catalyzed Reaction of 1-Alkenylboranes with 1-Alkenyl or 1-Alkynyl Halides. *Tetrahedron Lett.* **1979**, *20*, 3437–3440.
- (29) Miyaura, N.; Suzuki, A. Stereoselective Synthesis of Arylated (*E*)-alkenes by the Reaction of Alk-1-enylboranes with Aryl Halides in the Presence of Palladium Catalyst. *J. Chem. Soc. Chem. Commun.* **1979**, 866–867.
- (30) Miyaura, N.; Sugimoto, H.; Suzuki, A. A Stereospecific Synthesis of Conjugated (*E*, *Z*)- and (*Z*, *Z*)-Alikadienes by a Palladium-Catalyzed Cross-Coupling Reaction of 1-Alkenylboranes with 1-Alkenyl Bromides. *Tetrahedron Lett.* **1981**, *22*, 127–130.
- (31) Miyaura, N.; Yanagi, T.; Suzuki, A. The Palladium-Catalyzed Cross-Coupling Reaction of Phenylboronic Acid with Haloarenes in the Presence of Bases. *Synth. Commun.* **1981**, *11*, 513–519.
- (32) Choi, S. M.; Lee, S.; Kim, Y.-J.; Lee, J. H.; Lee, S. W.; Choi, J.-C. Bis(azido)palladium(II) Complexes Bearing an (*R* or *S*)-(BINAP) Ligand: Synthesis, Structures, and Catalytic Application to Suzuki–Miyaura C–C Coupling Reactions. *Bull. Korean Chem. Soc.* **2020**, *41*, 216–219.
- (33) Miyaura, N.; Suzuki, A. Palladium-Catalyzed Cross-Coupling Reactions of Organoboron Compounds. *Chem. Rev.* **1995**, *95*, 2457–2483.